Current Applied Physics 32 (2021) 106–110

Contents lists available at ScienceDirect

Current Applied Physics

journal homepage: www.elsevier.com/locate/cap

Nonlinearity in inverse and transverse piezoelectric properties of Pb($Zr_{0.52}Ti_{0.48}$)O_3 film actuators under AC and DC applied voltages

Minh D. Nguyen [a,b,c,*], Hung N. Vu [c,**], Guus Rijnders [a]

[a] MESA+ Institute for Nanotechnology, University of Twente, P.O. Box 217, 7500AE, Enschede, the Netherlands
[b] Solmates B.V., Auke Vleerstraat 3, 7521 PE, Enschede, the Netherlands
[c] International Training Institute for Materials Science (ITIMS), Hanoi University of Science and Technology, 1 Dai Co Viet Road, Hanoi, Viet Nam

ARTICLE INFO

Keywords:
Domain-wall motion
Piezoelectric coefficient
Nonlinearity
Piezoelectric film

ABSTRACT

The motion of domain walls is a crucial factor in piezoelectric properties and is usually related to the irreversible and hysteretic behaviors. Herein, we report on the investigation of inverse and transverse piezoelectric coefficients of capacitor-based and microcantilever-based Pb($Zr_{0.52}Ti_{0.48}$)O_3 films with a change in the DC bias and the AC applied voltage. A large inverse piezoelectric strain coefficient of about 350 p.m./V, and a low strain hysteresis of about 7.1%, are achieved in the film capacitors under a low applied voltage of 2 V (20 kV/cm) which can benefit the actuators for motion control in high-precision systems. The field-dependences of the transverse piezoelectric coefficients, obtained from four-point bending and microcantilever displacement, are in good agreement with each other. The results also reveal that the irreversible domain-wall motion is attributed to the nonlinearity in the field-dependent piezoelectric strain and cantilever displacement.

1. Introduction

In polycrystalline ferroelectric materials, the dielectric and piezoelectric properties are dependent on both intrinsic and extrinsic effects [1–4]. The intrinsic contributions originate from the atomic displacements (deformation) within each unit-cell of the ferroelectric material under an applied electric field, whereas the extrinsic contributions are related to the movement of the ferroelectric domain walls [5,6]. In ferroelectric perovskites, domain-wall motion can be of 180° or non-180° (90° in the tetragonal case, and 71° or 109° in the rhombohedral case). The movement of non-180° domain walls implies a change in both the ferroelastic (piezoelectric) and ferroelectric (polarization and dielectric constant) responses, meanwhile 180° domain walls are only ferroelectrically active [2,5,7–9]. Due to the presence of their complex grain and domain structure, the polycrystalline ferroelectric materials have a nonlinear behavior, while a linear behavior is expected for a single crystal [10]. The nonlinearity from the intrinsic effect is very small and is almost directly related to the extrinsic contribution [4,11]. On the other hand, the motion of the domain-walls induces hysteretic and nonlinear dielectric and piezoelectric properties. Moreover, previous reports have indicated that the piezoelectric-electric field dependence is almost linear (non-hysteric) at lower fields, and becomes nonlinear (hysteric) at higher fields, which is attributed to factors such as reversible domain-wall motion [7,12–16]. Under low electric fields the domain wall motion is expected to be reversible, and therefore, the field-induced atomic displacement within the unit cell contributes to the reversible component of the total piezoelectric displacement. Meanwhile, higher electric fields (which exceed the coercive field) are required to switch the non-180° domain-walls and then a larger piezoelectric strain generated per unit of applied electric field is expected. Generally, the piezoelectric response (d_{ij}) of a ferroelectric material due to motion of domain-walls can be described in terms of the Rayleigh model [2,15,17,18]:

$$d_{ij} = d_{init} + \alpha_d E_0 \quad (1)$$

where d_{init}, α_d and E_0 are the initial reversible piezoelectric response at zero electric field, the piezoelectric Rayleigh coefficient, and the amplitude of the applied electric field, respectively. The magnitude of $\alpha_d E_0$ presents the contribution of the domain-wall irreversible motion to the piezoelectric properties.

While the nonlinear hysteresis is a major limitation for some specific applications of piezoelectric actuators such as high-accuracy precision

* Corresponding author. MESA+ Institute for Nanotechnology, University of Twente, P.O. Box 217, 7500AE, Enschede, the Netherlands.
** Corresponding author.
E-mail addresses: d.m.nguyen@utwente.nl (M.D. Nguyen), hung.vungoc@hust.edu.vn (H.N. Vu).

https://doi.org/10.1016/j.cap.2021.10.007
Received 11 April 2021; Accepted 18 October 2021
Available online 26 October 2021

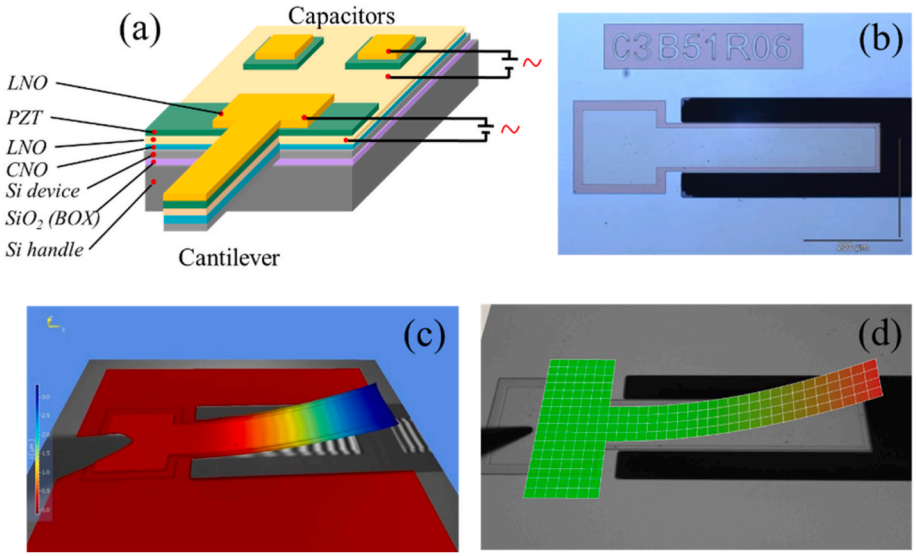

Fig. 1. (a) Capacitor and cantilever structures. (b–d) Microscope image, initial bending using white-light interferometer (WLI) and 3D-upward displacement using laser Doppler vibrometer (LDV), of a microcantilever. The length and width of microcantilever are 400-μm and 100-μm, respectively.

positioning via undesirable oscillations [19,20], it may also be useful in other applications like smart actuator devices, and as nonlinear oscillation based piezoelectric energy harvesters in which their inherent ability to improve the off-resonance performance (for instance, larger power output over a wide frequency range) compared to a similar linear resonant systems [21,22]. Therefore, further understanding of the nonlinear behavior underlying piezoelectricity is essential, not only from the scientific point of view, but also to help the development of industrial applications such as piezoelectric-assisted smart structures [23–25].

The scope of this study is to investigate the non-linearity in the reverse and transverse piezoelectric properties of textured Pb $(Zr_{0.52}Ti_{0.48})O_3$ (PZT) films, and their microcantilevers. In this work, the variation of the piezoelectric coefficient with change in applied voltage (AC and DC) has been characterized to show the contribution of domain wall motion to the field-induced piezoelectric strain (reverse piezoelectric coefficient) and the transverse piezoelectric coefficient.

2. Experimental

Ferroelectric $Pb(Zr_{0.52}Ti_{0.48})O_3$ (PZT) films, 1000-nm-thick, were grown on 100-nm-thick $LaNiO_3$ (LNO) oxide-electrodes buffered $Ca_2Nb_3O_{10}$-nanosheet/SOI (silicon-on-insulator) wafers using the pulsed laser deposition (PLD) method with a KrF excimer laser source (Lambda Physik, 248 nm wavelength). The $Ca_2Nb_3O_{10}$ (CNO) nanosheet, with a thickness of about 2.7 nm, was deposited on the SOI wafer using the Langmuir–Blodgett deposition method and was used as a surface template for highly (001)-oriented perovskite films on silicon [26]. The deposition conditions of the PZT and LNO layers have been presented in Ref. [27].

The process for fabricating piezoelectric driven Si microcantilevers has been described in a previous paper [28], and is shown schematically in Fig. 1. The cantilever structures, with a beam dimension of about 400-μm × 100-μm, consist of a LNO/PZT/LNO piezoelectric stack on CNO/SOI. The 10-μm-thick Si device (supporting layer) was obtained by backside etching of the SOI wafer.

The crystalline structure of the thin films was analyzed by X-ray diffraction θ-2θ scans (Philips X'Pert diffractometer). The microstructure was investigated by high-resolution scanning electron microscopy (HRSEM, Zeiss 1550). The polarization hysteresis (*P-E*) loop measurements were carried out using the ferroelectric mode of the aixACCT TF-2000 Analyzer with a triangular AC-voltage of ±20 V at 1 kHz scanning

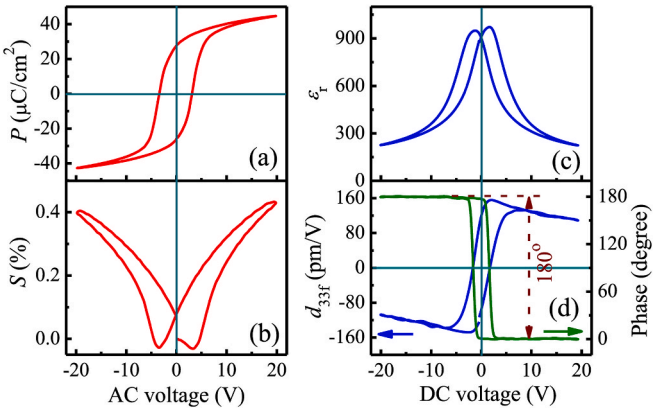

Fig. 2. AC voltage dependence (large-signal condition) of (a) polarization (*P–V*) and (b) piezoelectric strain (*S–V*). DC voltage dependence (small-signal condition) of (c) dielectric constant (ε_r-*V*) and (d) phase and inverse effective piezoelectric coefficient (d_{33f}-*V*).

frequency. The longitudinal piezoelectric coefficient ($d_{33,f}$) of the piezoelectric thin-film capacitor structures was measured by a Double Beam Laser Interferometer (aixDBLI) using a locked-in technique with a DC bias-driving between ± 20 V, with an AC amplitude of 0.4 V and 1 kHz frequency. The transverse piezoelectric coefficient $d_{31,f}$ was determined from the tip-displacement of the cantilevers, driven by the piezoelectric stack with an AC-amplitude of 1 Vp-p (peak-to-peak), 8 kHz frequency (much smaller than the natural resonant frequency of the prepared cantilevers of about 72 kHz), and various bias fields (−10 V to + 10 V DC-voltage).

3. Results and discussion

Fig. 2(a) and (b) present the *ac*-voltage dependence (dynamic measurement) of the polarization (*P–V*) loop and the piezoelectric strain (*S–V*) curve. The remanent polarization (P_r), maximum strain (S_m = 0.42%), and the normalized strain coefficient ($d^*_{33} = S_m t/V_m$, where *t* is PZT film thickness and V_m is maximum applied voltage) are 25.6 μC/cm^2, 0.42%, and 210 p.m./V, respectively. Fig. 2(b) shows that a difference in strain response under positive and negative applied voltage can be observed. In this case, the higher strain is observed under a

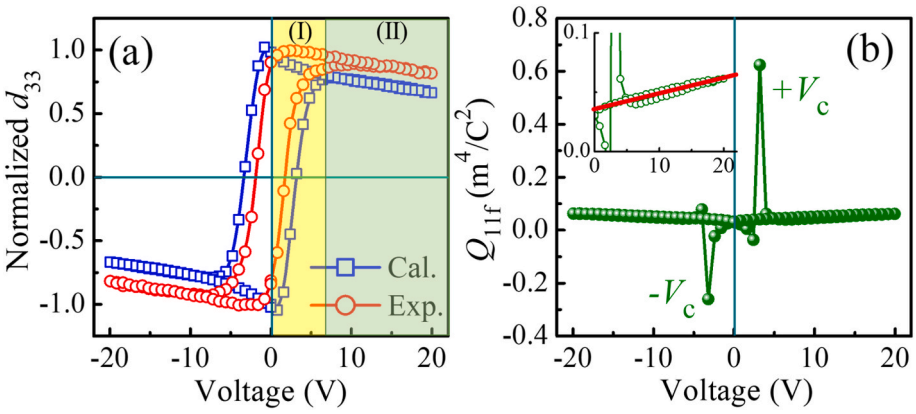

Fig. 3. (a) Comparison of calculated and experimental results of d_{33}-V loops and (b) effective inverse electrostriction coefficient-voltage (Q_{11f}-V) curve, as a function of applied voltage.

positive voltage which is in accordance with the film expanding away from the substrate, whereas the lower strain under a negative voltage is attributed to the constraint of the substrate [29]. Meanwhile, the dielectric constant ($\varepsilon_{r,0V}$) and the effective piezoelectric coefficient (d_{33f}), obtained from the *dc*-voltage dependence (static measurement) of the dielectric constant (ε_r-V) curve (Fig. 2(c)), and the piezoelectric (d_{33f}-V) loop (Fig. 2(d)), are 910 and 156 p.m./V, respectively. The change in d_{33f} value at the coercive voltage (Fig. 2(d)) occurs simultaneously with the domain switching observed in the ε_r-V curve (Fig. 2(c)). Fig. 2(c)-(d) also show that the ε_r and d_{33f} values increase with increasing applied voltage in the low-voltage region. In this region, more reversible domain-wall motion is activated with the increasing driving voltage which contributes to the enhancement of the ε_r and d_{33f} values. The maximum contribution of reversible domain-walls occurs around the coercive field (V_{sc}: small-signal coercive voltage) due to the maximal domain-wall density and mobility in which the peaks in the ε_r-V curve and d_{33f}-V loop are observed. On the other hand, the ε_r and d_{33f} values at low voltages are mainly contributed by domain-wall motion. However, due to the reduction of domain-wall density, the ε_r and d_{33f} values decrease as the driving voltage increases beyond the coercive field and the ε_r and d_{33f} values are now mainly associated with the intrinsic contribution [30,31]. The 180° phase switching shown in Fig. 2(d) indicates the existence of 180° domain walls, and the change in domain switching under applied voltage is generally associated with a purely ferroelectric character [30,32–34]. Meanwhile, the ε_r and d_{33f} values of $Al_{0.7}Sc_{0.3}N$ (ScAlN) films are found to be independent of DC bias (Fig. S3 (a)), indicating that only the lattice contribution has to be considered.

Moreover, Fig. 2(b) and (d) indicate that the small-signal d_{33f} value (156 p.m./V) is lower than that of the d^*_{33} value (210 p.m./V) measured with large-signal conditions. The lower d_{33f} value is caused by a reversible (intrinsic) effect, while the large-signal d^*_{33} value is governed by both reversible and irreversible (extrinsic) effects [35].

A theoretical calculation of the inverse piezoelectric coefficient (d_{33}) can be determined using the following equation:

$$d_{33} = 2Q_{11}\varepsilon_0\varepsilon_r P_3 \quad (2)$$

where Q_{11} is the inverse electrostriction coefficient, ε_0 (= 8.85 × 10^{-12} F/m) is the vacuum dielectric constant, ε_r is the dielectric constant of the film, and P_3 is the polarization in the direction of the polar axis. As shown in Fig. 3(a), a similar behavior of normalized d_{33}-E loops is observed between the theoretical and experimental values. In this theoretical calculation, the Q_{11} value is assumed to be independent of the applied voltage. However, Fig. 3(b) shows the applied voltage dependence of the effective inverse electrostriction coefficient (Q_{11f}) derived using Eq. (2) and based on the experimental data presented in Fig. 2(a), (c) and 2(d). Fig. 3(b) *inset* indicates that the Q_{11f} is slightly

Table 1
Comparison of coercive voltage defined from different measurements.

Measurement	V_{c+} (V)	V_{c-} (V)	Remark
P–V	3.21	−3.18	AC dynamic (large-signal)
C–V	1.71	−1.67	DC static (small-signal)
d_{33}-V (Exp)	1.71	−1.67	DC static (small-signal)
d_{33}-V (Cal)	3.16	−3.12	Mixed AC & DC
Q_{eff}-V (Cal)	3.28	−3.22	Mixed AC & DC

* Experiment (Exp) and Calculation (Cal).

increased with increasing applied voltage (Q_{11f} values are about 0.034 m^4/C^2 at zero bias and 0.061 m^4/C^2 at 20 V), except for the irregularities near the coercive voltages ($\pm V_c$). The divergence of the Q_{11f}-V curve around the coercive voltages can be as a result of different coercive voltages achieved from the P-E loop and d_{33f}-V (and ε_r-V) curve. Moreover, Fig. 3(a) also shows that both experimental and calculated d_{33} values reach a peak around/near zero voltage (region I) and then decrease with increasing applied voltage. This is mostly due to the abrupt decrease of the dielectric constant at high voltages (region II), which can be reasonably explained in terms of the clamping (or pinning) of domain walls by applying a DC bias voltage. The comparison of coercive voltage defined from different measurements is presented in Table 1.

As the most commonly applied electric-field type for piezoelectric devices in actuator applications is the unipolar driving mode, the unipolar field-induced strains (S_{uni}) of film capacitors under different driving voltages were considered and are presented in Fig. S2. The S_{uni}-V curve is almost linear at low applied voltage, in which the forward and backward curves are nearly overlapping (Fig. S2(a)). At higher applied voltages, nonlinear effects become apparent in the S_{uni}-V curves (Fig. S2 (b)-S2(d)), which are contributed to by factors such as domain-wall motion. To find an explanation for this relationship, the difference in domain-wall motion can be considered. While the piezoelectric response is based on the hypothesis that the displacement of domain walls is reversible (independent of applied voltages) at a low applied voltages, the domain-wall motion becomes partially irreversible, and results in the response of a unipolar piezoelectric strain at higher applied voltages [36].

It can be seen from Fig. 4(a) that the maximum strain ($S_{uni,m}$) values, achieved from Fig. S2, gradually increase with increasing applied voltage, reaching a $S_{uni,m}$ value of 0.42% at 20 V (or 200 kV/cm). Interestingly, the rising slope of the $S_{uni,m}$ values is different with changing applied voltage, where the rising slope measured under the low-voltage region (until 5 V) is larger than that measured under the high-voltage region (beyond 5 V). The difference in the rising slope in this study is dominated by the deformation of each unit cell under low

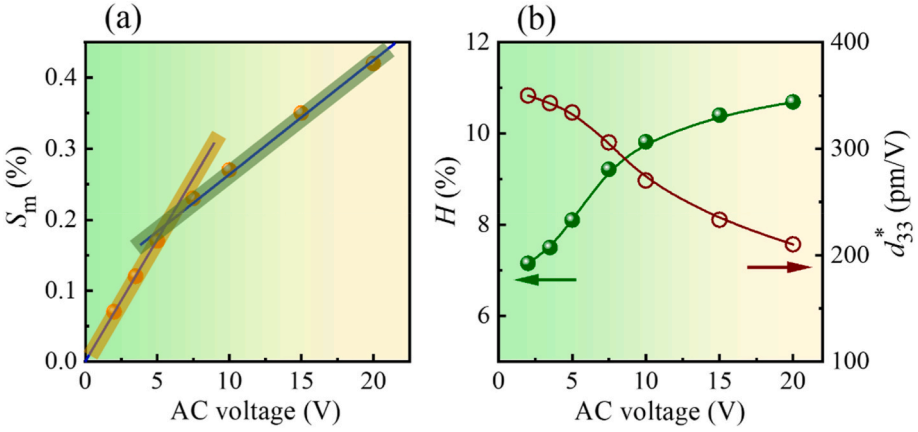

Fig. 4. (a) Unipolar maximum strain, and (b) normalized d_{33}^* and strain hysteresis (H) values, of PZT film capacitors at different driving voltages.

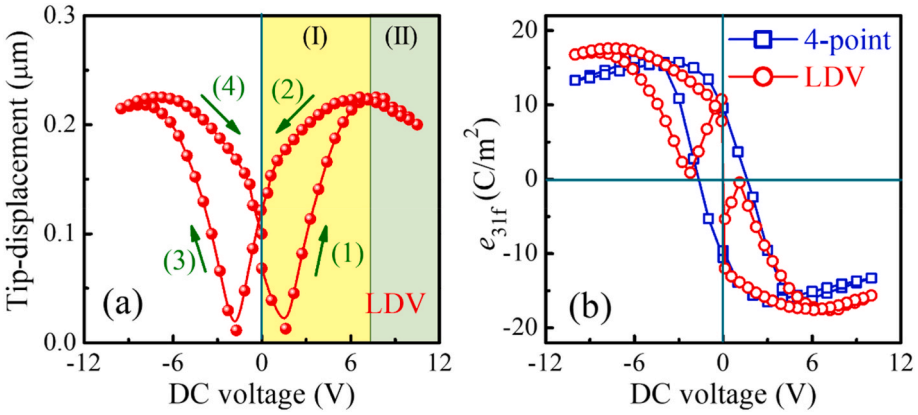

Fig. 5. DC voltage dependence of the (a) tip-displacement of cantilever using LDV and (b) e_{31f} values calculated from tip-displacement using LDV and obtained from four-point bending measurements.

voltages, and by domain-wall motion under high voltages, as discussed above. Moreover, due to the limitation of domain walls (or the domain walls are partly clamped), the normalized d_{33}^* value decreases with increasing applied voltage (Fig. 4(b)). In addition, the reversibility of the field-induced phase transition under low applied voltages can also produce the minimum irreversible strain for a larger d_{33}^* value, while the strain is mostly dominated by domain switching under high applied voltages [37,38]. The effect of field-induced domain-wall motion and switching can also be seen in the strain hysteresis (Fig. 4(b)), as calculated from the S_{uni}-V curves shown in Fig. S2d. The strain hysteresis (H) is small for low applied voltages and becomes larger as the applied voltage is increased, which is related to the irreversible domain-wall motion at higher applied voltages, as discussed in the previous section.

Fig. 5(a) shows the tip-displacement (δ_T) of the PZT microcantilever as a function of the bias voltage using the laser Doppler vibrometer (LDV) method. In this measurement, an AC-voltage of 1 Vp-p (peak-to-peak) was applied on a sweeping DC bias (0 → +10 V 'step 1' → −10 V 'steps 2–3' → 0 'step 4') and the piezoelectric displacement of the cantilever was measured at each bias step. The results indicate that the δ_T of the cantilever has a butterfly curve in which the polarity of the piezoelectric material is inverted near its coercive voltage (~1.7 V), so changing the direction of displacement, and the displacement becomes larger with the bias voltage. The significant hysteresis on sweeping DC bias voltage is consistent with the alignment of the ferroelectric domains [39]. Similar to the d_{33f}-V curve, the δ_T value first increases with increasing voltage (step 1), approaches the saturation value (0.225 μm/1Vac) at a bias voltage of 7.1 V, then decreases slightly with further increases in bias voltage. This behavior can also be attributed to large extrinsic effects (domain-wall motion) that has been discussed in a previous section. However, the $Al_{0.7}Sc_{0.3}N$ (ScAlN) films-based microcantilevers do not exhibit a hysteresis loop due to the absence of ferroelectric domains (Fig. S3(b)).

Fig. 5(b) compares the effective transverse piezoelectric coefficient (e_{31f}) values calculated from the tip-displacement of PZT microcantilevers using LDV (the calculation was presented in Ref. [40] and in Supporting Information), and those obtained from the four-point bending (FPB) measurements [41,42]. The shapes of both $e_{31,f}$-V curves are in good agreement. The values of the coercive voltages and the slopes of their curves are similar in both cases. However, the maximum (saturated) e_{31f} values are not equal due to the different measurement conditions for both methods, with the maximum e_{31f} values being −17.6 and −16.4 C/m^2 with the LDV and FPB methods, respectively.

4. Conclusions

Nonlinearity analysis is a useful process for studying the domain wall contribution in ferroelectric materials as well as for understanding the role that extrinsic contributions play in the piezoelectric properties. The hysteretic strain-voltage and cantilever displacement-voltage loops, with a typical butterfly-like shape, were achieved in the PZT film capacitors and PZT film microcantilevers. This can be attributed to the domain-wall reversal where mainly non-180° rather than 180° domain-wall reversal contributes to the strain and cantilever displacement. Moreover, a large normalized d_{33}^* value of 350 p.m./V, and a low strain hysteresis of 7.1%, were achieved under a low applied voltage of 2 V (20

kV/cm) due to the minimum irreversible strain attributed under low applied voltages. The findings in this study may provide a framework for the understanding of the contribution of domain wall motion to the piezoelectric responses of capacitor and cantilever structures, which is expected to benefit the development of piezoelectric films in high-precision displacement control systems.

Declaration of competing interest

The authors declare that they have no known competing financial interests or personal relationships that could have appeared to influence the work reported in this paper.

Acknowledgements

The authors would like to acknowledge the financial support from the National Foundation for Science and Technology Development (NAFOSTED) of Vietnam under Grant No. 103.99–2018.23.

Appendix A. Supplementary data

Supplementary data to this article can be found online at https://doi.org/10.1016/j.cap.2021.10.007.

References

[1] C.A. Randall, N. Kim, J.P. Kucera, W. Cao, T.R. Shrout, Intrinsic and extrinsic size effects in fine-grained morphotropic-phase-boundary lead zirconate titanate ceramics, J. Am. Ceram. Soc. 81 (1998) 677–688.
[2] Q.M. Zhang, H. Wang, N. Kim, L.E. Cross, Direct evaluation of domain-wall and intrinsic contributions to the dielectric and piezoelectric response and their temperature dependence on lead zirconate-titanate ceramics, J. Appl. Phys. 75 (1994) 454–459.
[3] C. Ang, Z. Yu, Dielectric behavior of $PbZr_{0.52}Ti_{0.48}O_3$ thin films: intrinsic and extrinsic dielectric responses, Appl. Phys. Lett. 85 (2004) 3821–3823.
[4] A. Benjeddou, Field-dependent nonlinear piezoelectricity: a focused review, Int. J. Smart Nano Mater. 9 (2018) 68–84.
[5] F. Xu, S. Trolier-McKinstry, W. Ren, B. Xu, Z.L. Xie, K.J. Hemker, Domain wall motion and its contribution to the dielectric and piezoelectric properties of lead zirconate titanate films, J. Appl. Phys. 89 (2001) 1336–1348.
[6] W. Wersing, W. Heywang, H. Beige, H. Thomann, The role of ferroelectricity for piezoelectric materials, in: W. Heywang, K. Lubitz, W. Wersing (Eds.), Piezoelectricity: Evolution and Future of a Technology, Springer Berlin Heidelberg, Berlin, Heidelberg, 2008, pp. 37–87.
[7] S. Trolier-McKinstry, N. Bassiri-Gharb, D. Damjanovic, Piezoelectric nonlinearity due to motion of 180° domain walls in ferroelectric materials at subcoercive fields: a dynamic poling model, Appl. Phys. Lett. 88 (2006) 202901.
[8] D. Damjanovic, Stress and frequency dependence of the direct piezoelectric effect in ferroelectric ceramics, J. Appl. Phys. 82 (1997) 1788–1797.
[9] D.J. Kim, J.P. Maria, A.I. Kingon, S.K. Streiffer, Evaluation of intrinsic and extrinsic contributions to the piezoelectric properties of $Pb(Zr_{1-x}Ti_x)O_3$ thin films as a function of composition, J. Appl. Phys. 93 (2003) 5568–5575.
[10] A. Albareda, R. Pérez, Non-linear behaviour of piezoelectric ceramics, in: L. Pardo, J. Ricote (Eds.), Multifunctional Polycrystalline Ferroelectric Materials: Processing and Properties, Springer Netherlands, Dordrecht, 2011, pp. 681–726.
[11] S. Li, W. Cao, L.E. Cross, The extrinsic nature of nonlinear behavior observed in lead zirconate titanate ferroelectric ceramic, J. Appl. Phys. 69 (1991) 7219–7224.
[12] I. Chopra, J. Sirohi, Smart Structures Theory, Cambridge University Press, 2014.
[13] R.E. Eitel, Rayleigh law response in ferroelectric ceramics: quantifying domain wall dynamics and structural relationships, in: Sixteenth IEEE International Symposium on the Applications of Ferroelectrics, 2007, pp. 319–323. Nara, Japan.
[14] P. Chen, R.J. Sichel-Tissot, J.Y. Jo, R. T Smith, S.H. Baek, W. Saenrang, C.B. Eom, O. Sakata, E.M. Dufresne, P.G. Evans, Nonlinearity in the high-electric-field piezoelectricity of epitaxial $BiFeO_3$ on $SrTiO_3$, Appl. Phys. Lett. 100 (2012), 062906.
[15] D.A. Hall, Review Nonlinearity in piezoelectric ceramics, J. Mater. Sci. 36 (2001) 4575–4601.
[16] D. Damjanovic, Nonlinear piezoelectric response in ferroelectric ceramics, in: C. Galassi, M. Dinescu, K. Uchino, M. Sayer (Eds.), Piezoelectric Materials: Advances in Science, Technology and Applications, Springer Netherlands, Dordrecht, 2000, pp. 123–135.
[17] R.E. Eitel, T.R. Shrout, C.A. Randall, Nonlinear contributions to the dielectric permittivity and converse piezoelectric coefficient in piezoelectric ceramics, J. Appl. Phys. 99 (2006) 124110.
[18] K. Kobayashi, Y. Doshida, Y. Mizuno, C.A. Randall, A route forwards to narrow the performance gap between PZT and lead-free piezoelectric ceramic with low oxygen partial pressure processed $(Na_{0.5}K_{0.5})NbO_3$, J. Am. Ceram. Soc. 95 (2012) 2928–2933.
[19] H. Ikeda, T. Morita, High-precision positioning using a self-sensing piezoelectric actuator control with a differential detection method, Sens. Actuators, A 170 (2011) 147–155.
[20] R.J.E. Merry, N.C.T. de Kleijn, M.J.G. van de Molengraft, M. Steinbuch, Using a walking piezo actuator to drive and control a high-precision stage, IEEE ASME Trans. Mechatron. 14 (2009) 21–31.
[21] V. Mueller, H. Beige, Nonlinearity of soft PZT piezoceramic for shear and torsional actuator applications, in: Proceedings of the Eleventh IEEE International Symposium on Applications of Ferroelectrics (Cat. No.98CH36245), Montreux, Switzerland, 1998, pp. 459–462.
[22] N.T. Beigh, P.S. Azad, P. Parkash, D. Mallick, High performance, nonlinear piezoelectric MEMS energy harvesting from low-threshold mechanical vibrations, in: 19th International Conference on Micro and Nanotechnology for Power Generation and Energy Conversion Applications (PowerMEMS), Krakow, Poland, 2019, 20515804804.
[23] J. Qiu, J. Ji, J. Liu, K. Zhu, Piezoelectric devices and their application in smart structures, in: Symposium on Piezoelectricity, Acoustic Waves, and Device Applications, 2008, pp. 416–422. Nanjing, China.
[24] M. Shirvanimoghaddam, K. Shirvanimoghaddam, M.M. Abolhasani, M. Farhangi, V.Z. Barsari, H. Liu, M. Dohler, M. Naebe, Towards a green and self-powered internet of things using piezoelectric energy harvesting, IEEE Access 7 (2019) 94533–94556.
[25] A. Nechibvute, A. Chawanda, P. Luhanga, Piezoelectric energy harvesting devices: an alternative energy source for wireless sensors, Smart Mater. Res. (2012) 853481.
[26] M.D. Nguyen, H. Yuan, E.P. Houwman, M. Dekkers, G. Koster, J.E. ten Elshof, G. Rijnders, Highly oriented growth of piezoelectric thin films on silicon using two-dimensional nanosheets as growth template layer, ACS Appl. Mater. Interfaces 8 (2016) 31120–31127.
[27] M.D. Nguyen, R. Tiggelaar, T. Aukes, G. Rijnders, G. Roelof, Wafer-scale growth of highly textured piezoelectric thin films by pulsed laser deposition for micro-scale sensors and actuators, J. Phys. Conf. Ser. 922 (2017), 012022.
[28] M.D. Nguyen, M. Dekkers, H.N. Vu, G. Rijnders, Film-thickness and composition dependence of epitaxial thin-film PZT-based mass-sensors, Sens. Actuators, A 199 (2013) 98–105.
[29] T.A. Berfield, R.J. Ong, D.A. Payne, N.R. Sottos, Residual stress effects on piezoelectric response of sol-gel derived lead zirconate titanate thin films, J. Appl. Phys. 101 (2007), 024102.
[30] J.P. de la Cruz, E. Joanni, P.M. Vilarinho, A.L. Kholkin, Thickness effect on the dielectric, ferroelectric, and piezoelectric properties of ferroelectric lead zirconate titanate thin films, J. Appl. Phys. 108 (2010) 114106.
[31] W. Gong, J.F. Li, X. Chu, Z. Gui, L. Li, Combined effect of preferential orientation and Zr/Ti atomic ratio on electrical properties of $Pb(Zr_xTi_{1-x})O_3$ thin films, J. Appl. Phys. 96 (2004) 590–595.
[32] A.L. Kholkin, E.K. Akdogan, A. Safari, P.-F. Chauvy, N. Setter, Characterization of the effective electrostriction coefficients in ferroelectric thin films, J. Appl. Phys. 89 (2001) 8066–8073.
[33] S.V. Kalinin, A.N. Morozovska, L.Q. Chen, B.J. Rodriguez, Local polarization dynamics in ferroelectric materials, Rep. Prog. Phys. 73 (2010), 056502.
[34] J. Stephen, A.P. Baddorf, S.V. Kalinin, Switching spectroscopy piezoresponse force microscopy of ferroelectric materials, Appl. Phys. Lett. 88 (2006), 062908.
[35] P. Gerber, C. Kügeler, U. Böttger, R. Waser, Effects of reversible and irreversible ferroelectric switchings on the piezoelectric large-signal response of lead zirconate titanate thin films, J. Appl. Phys. 98 (2005) 124101.
[36] D. Lin, S. Zhou, W. Liu, F. Li, Thermal stability and electric-field-induced strain behaviors for PIN-PSN-PT piezoelectric ceramics, J. Am. Ceram. Soc. 101 (2018) 316–325.
[37] J. Fu, R. Zuo, H. Qi, C. Zhang, J. Li, L. Li, Low electric-field driven ultrahigh electrostrains in Sb-substituted $(Na,K)NbO_3$ lead-free ferroelectric ceramics, Appl. Phys. Lett. 105 (2014) 242903.
[38] X. Lv, J. Wu, D. Xiao, Y. Yuan, H. Tao, J. Zhu, X. Wang, X. Lou, High unipolar strain in samarium-doped potassium–sodium niobate lead-free ceramics, RSC Adv. 5 (2015) 39295–39302.
[39] B. Jaffe, W.R. Cook, H.L. Jaffe, Piezoelectric Ceramics, Academic Press, London, 1971.
[40] M. Dekkers, H. Boschker, M. van Zalk, M. Nguyen, H. Nazeer, E. Houwman, G. Rijnders, The significance of the piezoelectric coefficient $d_{31,eff}$ determined from cantilever structures, J. Micromech. Microeng. 23 (2012), 025008.
[41] Y. Tsujiura, S. Kawabe, F. Kurokawa, H. Hida, I. Kanno, Comparison of effective transverse piezoelectric coefficients $e_{31,f}$ of $Pb(Zr,Ti)O_3$ thin films between direct and converse piezoelectric effects, Jpn. J. Appl. Phys. 54 (2015) 10NA04.
[42] K. Prume, P. Muralt, T. Schmitz-Kempen, S. Tiedke, Tensile and compressive stress dependency of the transverse ($e_{31,f}$) piezoelectric coefficient of PZT thin films for MEMS devices, in: SPIE Smart Structures and Materials + Nondestructive Evaluation and Health Monitoring, vol. 6526, SPIE, 2007, 65260G(1-12).